Passive Transduction Features of Skin

NE 466 Tactical Sensors and Transducers

Faculty of Engineering - Nanotechnology Engineering Program

Group 5

Andrew Wang - 20876295

Mathew Maradin - 20877924

Michael Hanley - 20877480

Randy Dakhil - 20894797

Rian Matti - 20882217

Table of Contents

1. Introduction

The human skin acts as the interface between the body and its environment, enabling the sense of touch through mechanically sensitive neurons known as mechanoreceptors [1]. The skin's structural properties passively enhance transduction by modulating external mechanical stimuli before they reach mechanoreceptor-containing layers of the skin. This modulation plays a crucial role in human tactile perception [2].

One important structural feature of the skin is the presence of epidermal ridges, known as fingerprints. Researchers have suggested that one of their various functions is to amplify mechanical stress [3]. When a fingertip touches a surface, the fingerprint ridges are deformed to conform to the surface's fine texture [4]. As a result, the stress distribution between the skin and the surface is modulated, amplifying the skin vibrations induced by surface features with periodicities similar to that of the fingerprint ridges [2]. Therefore, the ridges act as mechanical filters and play a key role in enhancing humans' ability to decipher fine surface textures and the precise encoding of tactile information [3].

The role of fingerprints in the encoding of tactile information has been studied using various methods, such as probing with a biomimetic sensor [5] and psychological experiments involving blocking tactile information at the fingertips [6]. However, if the mechanics of fingerprint and skin deformations, fingerprint structure, and mechanoreceptor responses are well understood, then the role of fingerprints can be studied much more efficiently using computational models and simulations.

This project aims to study the effect of passive transduction features of skin in tactile encoding using simulations developed in Python, with a particular focus on the fingerprint ridges and modeling them using different geometric profiles.

2. Background

2.1 Structure of Skin

Skin is a composite material composed of two layers—the epidermis and the dermis—each with different structures and functions. These layers consist of various biopolymers, with the outer epidermis layer of the skin primarily containing keratin and actin filaments. The inner dermis layer consists of collagen and elastic fibres, with their relative proportions varying across its thickness. The skin exhibits viscoelastic behaviour due to the behaviour of collagen and elastic fibres, where collagen primarily contributes to elasticity of the skin and elastic fibres exhibit more viscous properties [7].

The epidermis contains the visible fingerprint ridges and enhances tactile sensitivity. The dermis houses most of the sensory receptors within it or at the interface between the two layers, playing a key role in the skin's mechanical response. These structural properties influence how external stimuli applied to the epidermis are transmitted to deeper sensory receptors [8][19].

2.2 Mechanoreceptors

Mechanoreceptors are sensory receptors that utilize mechanically-gated ion channels to convert extracellular stimulus into intracellular signals. This process enables the transduction of touch, pressure, stretching, sound, motion, and other mechanical forces [9].

There are four main categories of mechanoreceptors, classified based on their adaptation properties (slow-adapting or fast-adapting) and depth within the skin (near-field or far-field). Slow-adapting (SA) receptors respond primarily to sustained stimuli while fast-adapting (FA) receptors respond to dynamic stimuli. Near-field (Type I) receptors are located in the dermis near the epidermal surface, allowing them to encode finer topographical features with a high spatial resolution and a local field of response. In contrast, far-field (Type-II) receptors are embedded deeper within the dermis, so they are more sensitive to macro-scale features and have a large area of response [10].

Knowing this, the properties of the four categories of receptors can be summarized:

1. Slow-adapting type I (SAI) receptors (*Merkel disks*): Detect sustained stimuli and have a well-defined, localized field of response, enabling the perception of sustained pressure [11].
2. Slow-adapting type II (SAII) receptors (*Ruffini Endings*): Detect sustained stimuli and have a large field of response, enabling perception of long-term strain such as skin stretching, movement, and finger positioning [11].
3. Fast-adapting type I (FAI) receptors (*Meissner Corpuscle*): Detect changes in stimuli and have a well-defined, localized field of response, primarily responding to dynamic deformation [11].
4. Fast-adapting type II (FAII) receptors (*Pacinian Corpuscle*): Detect changes in stimuli and have a large field of response, primarily sending vibrations and finer texture details.

The locations of the different receptors within the cross-section of skin are illustrated in Figure 1.

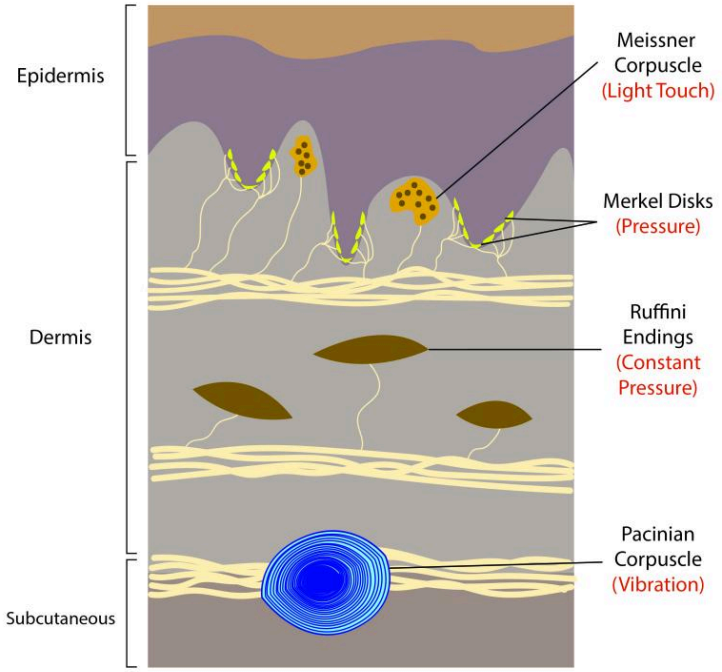

Figure 1. A cross-section of human skin showing the location of the four main types of mechanoreceptors within its layers. Each mechanoreceptor is associated with a different type of stimuli [11].

2.3 Epidermal Ridges

There are three main types of epidermal ridges on our fingertips, palms, and soles. These are whorls, loops, and arches, and are characterized based on their ridge structure and the direction the ridges converge to each other. Loops are the most common pattern for fingerprint ridges, where ridges curve back and exit on the same side. Whorls have spiral-like patterns with ridges forming complete loops. Arches have the simplest ridge structure relative to the other patterns, with an almost "flat" structure due to their gentle wave without any looping [12]. In modelling the different types of fingerprint ridges in this report, simplifications are made to the curvatures of the ridges. Loops are represented using a sinusoidal pattern due to their repeating motion in curving back on themselves and exiting on the same side, despite them not being perfect sine waves. Whorls are modelled using a spiral due to their circular ridge formation, though not all whorls are spirals and can be more oval-shaped or have more irregular looping patterns. Arches lack loops and only have a smooth, wave-like appearance, and can be reduced down to a flat profile.

2.4 Kelvin-Voigt Model

A Kelvin-Voigt material is a simple model viscoelastic material, with a viscoelastic response similar to that of an entangled polymer [13]. The model consists of a purely viscous dashpot and a purely elastic spring connected in parallel, as shown in Figure 2 below [14].

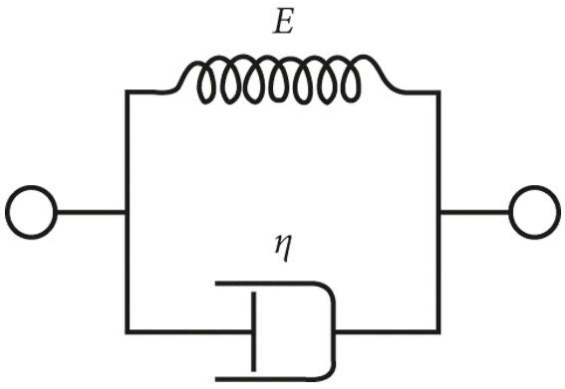

Figure 2. A schematic representation of the Kelvin-Voigt model, consisting of a purely viscous dashpot and purely elastic spring connected in parallel [14].

The two components will experience the same strain, as they are arranged in parallel. The total stress will be the sum of the stress in each component. Therefore, the basic equation for a Kelvin-Voigt element can be described below [13].

$$\sigma = E\epsilon + \eta\frac{d\epsilon}{dt}$$

Another model that was considered was the Maxwell model, which consists of the same elements as seen in Figure 2, but in a series connection rather than parallel. This model is better at handling stress relaxation but fails at accounting for creep. This is the opposite problem for the Kelvin-Voigt model. For this experiment, the model will undergo constant stress after some time value, so the Kelvin-Voigt model will be a better representation of the human skin's creep handling.

2.5 Previous Studies

Previous studies have done physical experiments to determine the mechanical response of human skin. For example, a study from the Journal of Ageing Science found that Young's modulus varies as the user increases in age [15]. One method of this effect is explained to be caused by the thickening of the skin in one's early years, decreasing the Young's modulus. The opposite occurs at an age above 80 years old. This effect will be tested in the simulation by varying the Young's modulus over the range specified by the paper.

3. Simulations

A Python-based simulation was developed to study the effect of fingertip ridges on tactile sensing, using libraries such as NumPy, SciPy, pandas, and Perlin noise for computation, as well as Matplotlib to generate the graphs shown in the following sections.

The simulation can be categorized into four high-level steps. Firstly, a matrix is created to model the skin's geographical features. Secondly, another matrix defines the pressure map

pattern, including a circular pattern, a linear pattern, and a singular point pattern. Next, the skin is treated as a Kelvin-Voigt material. Using this assumption, the deformation of the skin is computed, along with some statistical properties of the skin after deformation. Lastly, the responses of the four mechanoreceptor types (SAI, SAII, FAI, and FAII) are calculated. The finite differences method was used to compute the first and second derivatives.

The simulation runs with a 0.01-second time step over a 10-second duration. The maximum and average displacement values are calculated and plotted over time for visualization. Receptor responses for specific points of interest around the affected region in the surface profile will be analyzed [16].

3.1 Passive Features of Skin

The simulation incorporates two key passive features of skin: the mechanical properties of skin and the structure of skin ridges (fingerprints). The mechanical properties of the skin are characterized by its elastic modulus and viscosity coefficient, which define how the skin deforms under applied pressure. The simulation assumes an elastic modulus (stiffness) of 1.54 MPa and a viscosity coefficient of 1 Pa·sec. The Young's modulus value was chosen from a study that was able to measure the modulus orthogonal to the finger ridges [17].

These values were chosen arbitrarily to just observe the relative effects of skin structures on mechanoreceptor response. However, they could be refined using literature-based values for a more accurate model. The viscosity coefficient in particular is highly variable, typically ranging from 0.1 - 2.5 Pa·sec for Kelvin-Voigt models. This variation is caused by several factors including age, environment temperature, and hydration amongst others resulting in the need to pick an arbitrary value for this simulation [18].

In terms of the structure of skin ridges, the model defines three different ridge structures: wave-like ridges, spiral ridges, and flat ridges. The ridge structures are generated using a matrix to represent the skin's surface and ridge height, with ridges modelled as mathematical functions

with added noise. In this model, Perlin noise is used, as it generates a smooth gradient-type of randomness, making the skin structures appear more natural instead of truly random [14].

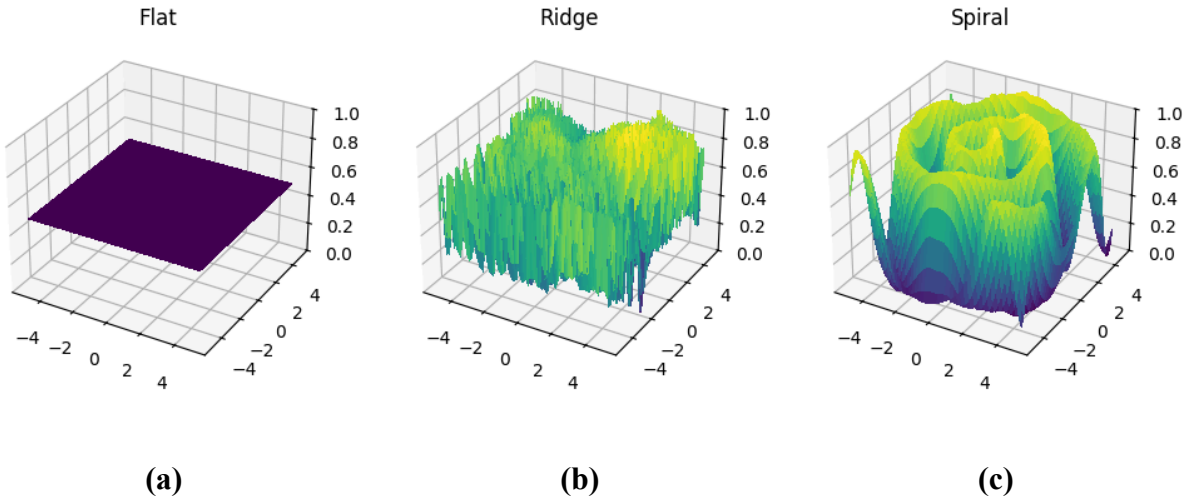

Figure 3. Structures generated for modelling different types of fingerprint ridges

In the case of the flat surface, the surface is uniform with a height of 0 everywhere (for all (x,y) coordinates), as seen above in Figure 3 (a). The wave-like ridges are generated by using a sine-based function with added Perlin noise, extending in both x and y directions, to mimic arches-like epidermal ridges, shown in Figure 3 (b). Lastly, the spiral-like ridge structures are generated using a sine function with a varying frequency/period (therefore a varying radius from the centre of the map) and a varying phase shift (varying angular coordinate from the centre of the map), resulting in a spiral-like pattern. Perlin noise distortion is also added to the spiral ridge, creating the structure shown in Figure 3 (c). These three structures will define the initial geometric profile of the skin.

3.2 Application of Pressure via Pressure Maps

Pressure maps are used to apply external forces to the skin. A function generates a 2D array representing the pressure distribution on a grid. In this model, the pressure map can be circular, point-based, or linear, which allows for the study of how different types of forces spread across different ridge structures. The function parameters include the grid dimensions/shape

(height and width), pattern type, central coordinates (x, y) of the pressure pattern, radius (for circular patterns) or width (for linear patterns), and maximum pressure intensity.

For a circular pattern, the function calculates the distance of each grid point from the centre and applies a pressure that decreases linearly with increasing distance. The radius parameter defines the maximum distance where the pressure is nonzero. The intensity parameter controls the maximum pressure, which is located at the centre.

To model a point-like pattern, pressure is applied at a single point at the centre, followed by a Gaussian filter that spreads the pressure outwards from the centre. The result is a smooth distribution around the central point, with the highest intensity of pressure at the centre and gradually decreasing outward. The radius parameter determines the standard deviation of the filter, affecting the spread of pressure.

Lastly, to model a linear pressure pattern, the pressure varies linearly along a specific row with the maximum intensity along the centre line (determined by the y-coordinate of the center). Pressure decreases smoothly to zero within a specified range, controlled by the radius parameter, which defines the rate of pressure decay from the central line.

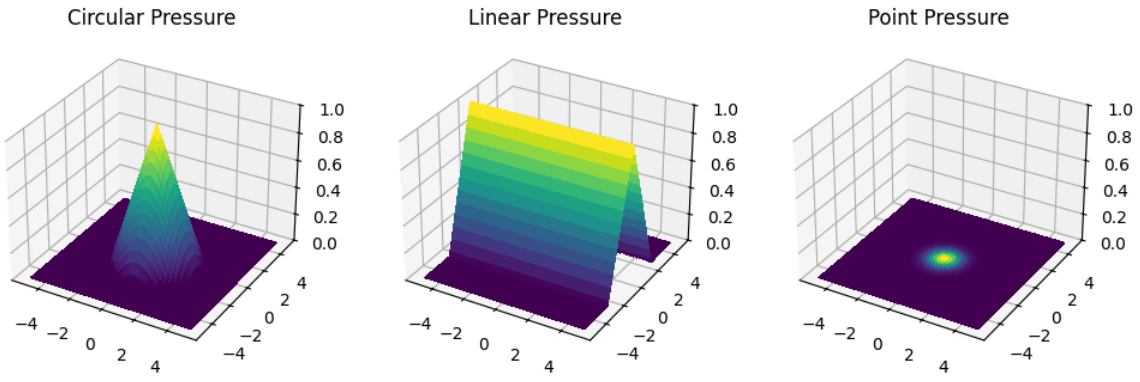

Figure 4. Different pressure maps will be applied to the generated finger ridges.

In the model, pressure maps are applied to the different ridge surfaces to analyze how different skin geometries affect force distribution. This approach enables the study of both localized and distributed forces, which is important for understanding how pressure variations influence tactile perception.

For this experiment, only the circular pressure pattern will be explored in depth. The other patterns will only be compared with each other via the displacement plots.

3.3 Modeling Deformation

To model the deformation over time, a Kelvin-Voigt viscoelastic representation is used to model the skin's response. This model combines elastic and viscous effects to compute the skin's deformation, strain, and curvature across a grid of points representing the skin's surface. This is done by iterating the deformation of the skin's surface using finite-difference methods, allowing for the analysis of how skin reacts to different stress patterns.

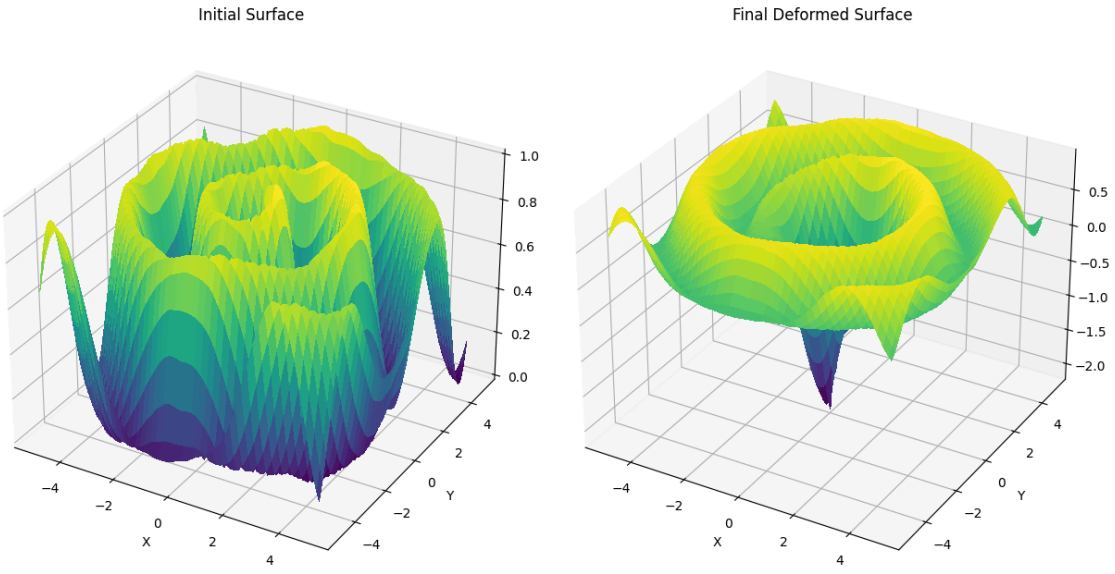

Figure 5. Model of skin surface before and after deformation using the Kelvin-Voigt model. This example uses spiral-like fingerprint ridges.

3.4 Modeling Mechanoreceptor Types

In the final step, the model calculates receptor responses based on the four mechanoreceptor types. SAI receptors respond to static deformation, SAII receptors respond to sustained deformation, FAI receptors respond to dynamic deformation rates, and FAII receptors respond to acceleration in deformation. The curvature of the surface profile is incorporated into these calculations. A higher curvature indicates the presence of a ridge, which may amplify the receptor response.

To calculate the SAI response from a deformation, the resulting strain is scaled by the curvature of the surface profile, following the equation shown below. If the surface profile is flat (possesses no curvature), the value of curvature will be set to 1.

$$SA_I = \epsilon(t) \times (1 + C)$$

For the SAII response, the cumulative sum of all strains up to a time is calculated. The accumulated strain is then scaled by the curvature of the surface profile, which ensures that regions with higher curvature, such as skin ridges, amplify the response. The equation shown below expresses this response.

$$SA_{II} = \int_0^t \epsilon(t)dt \times (1 + C)$$

Since the FA receptor response depends primarily on the rate of change of the stress, their responses will require the computation of the derivatives using finite difference equations. However, for the first derivative, the Kelvin-Voigt equation is applied. Similar to SA receptors, the response of FA receptors are also scaled by the curvature of the surface profile to account for the amplification effect in regions with higher curvature.

$$FA_I = \frac{d\epsilon(t)}{dt} \times (1 + C) = \frac{\sigma - E\epsilon(t)}{\eta} \times (1 + C)$$

For the FAII receptor, the second derivative is used. It was calculated from the first derivative using the first-order central difference formula. This is also adjusted with the local curvature. Therefore, the formula for this response is provided below.

$$FA_{II} = \frac{d^2\epsilon(t)}{dt^2} \times (1 + C) = \frac{\frac{d\epsilon(t+1)}{dt} - \frac{d\epsilon(t-1)}{dt}}{2\Delta t} \times (1 + C)$$

The curvature at every point on the deformed surface (D) and at every time step is calculated by computing the second derivative in both the x and y directions. Both of these values are summed to get the C value as shown in the expression below.

$$C = \Delta^2 D_x + \Delta^2 D_y$$

4. Results & Analysis

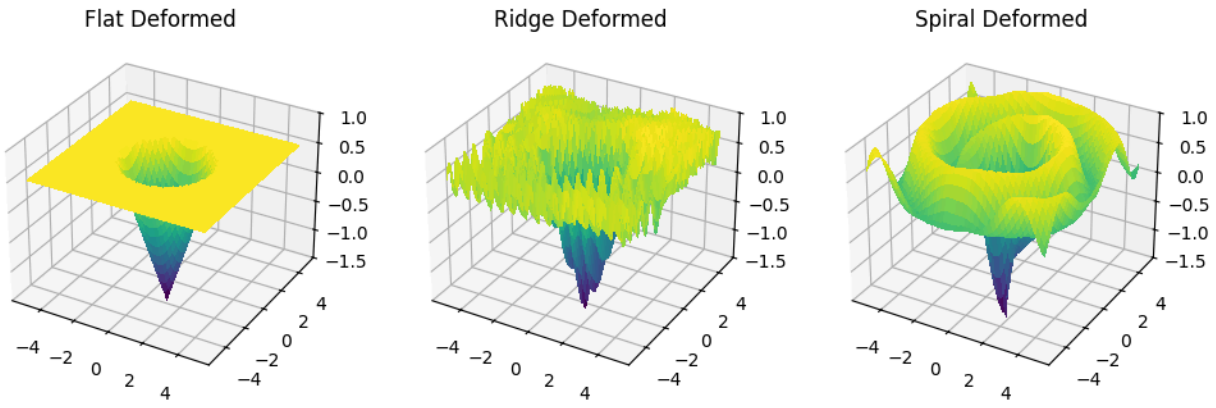

Figure 6. Deformed surfaces with the circular pressure pattern at maximum intensity.

For each of the pressure maps, their displacement differs vastly. From the flat surface profile, the maximum and average displacement from each of the pressure maps have their differences and similarities. Between the circular and the linear pressure maps, they have a similar maximum displacement but vary in their average displacement. This indicates that the linear pressure map will cause more displacement than the spherical map. For the point pressure, due to its low pressure, the maximum and average displacement are lower than the rest.

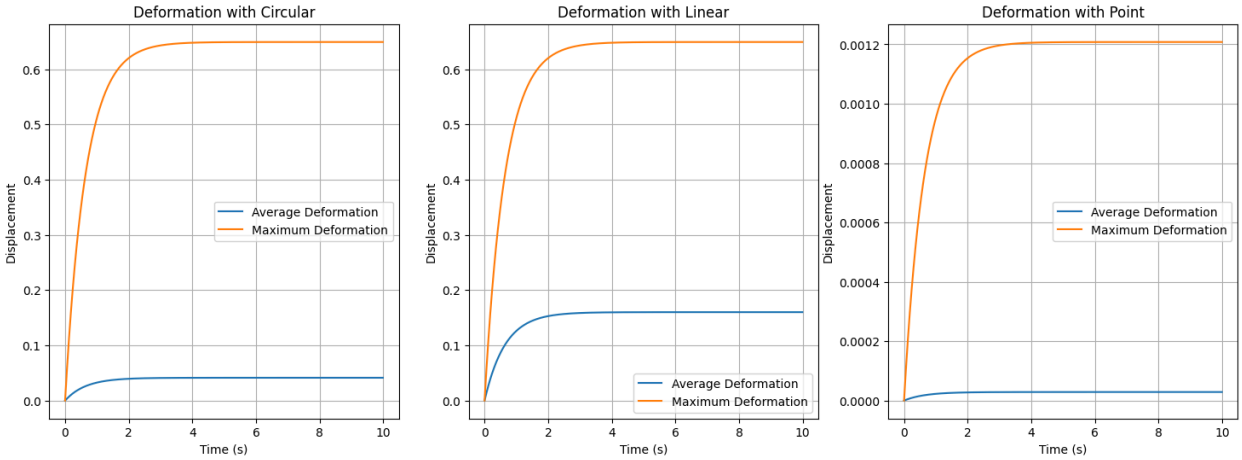

Figure 7. Maximum and average displacement for each different pressure map.

Based on the results of the simulation, the response from the receptors does match up to their theoretical behaviour. From the flat and ridge surface profiles, the application of the circular pressure map generated the following receptor responses.

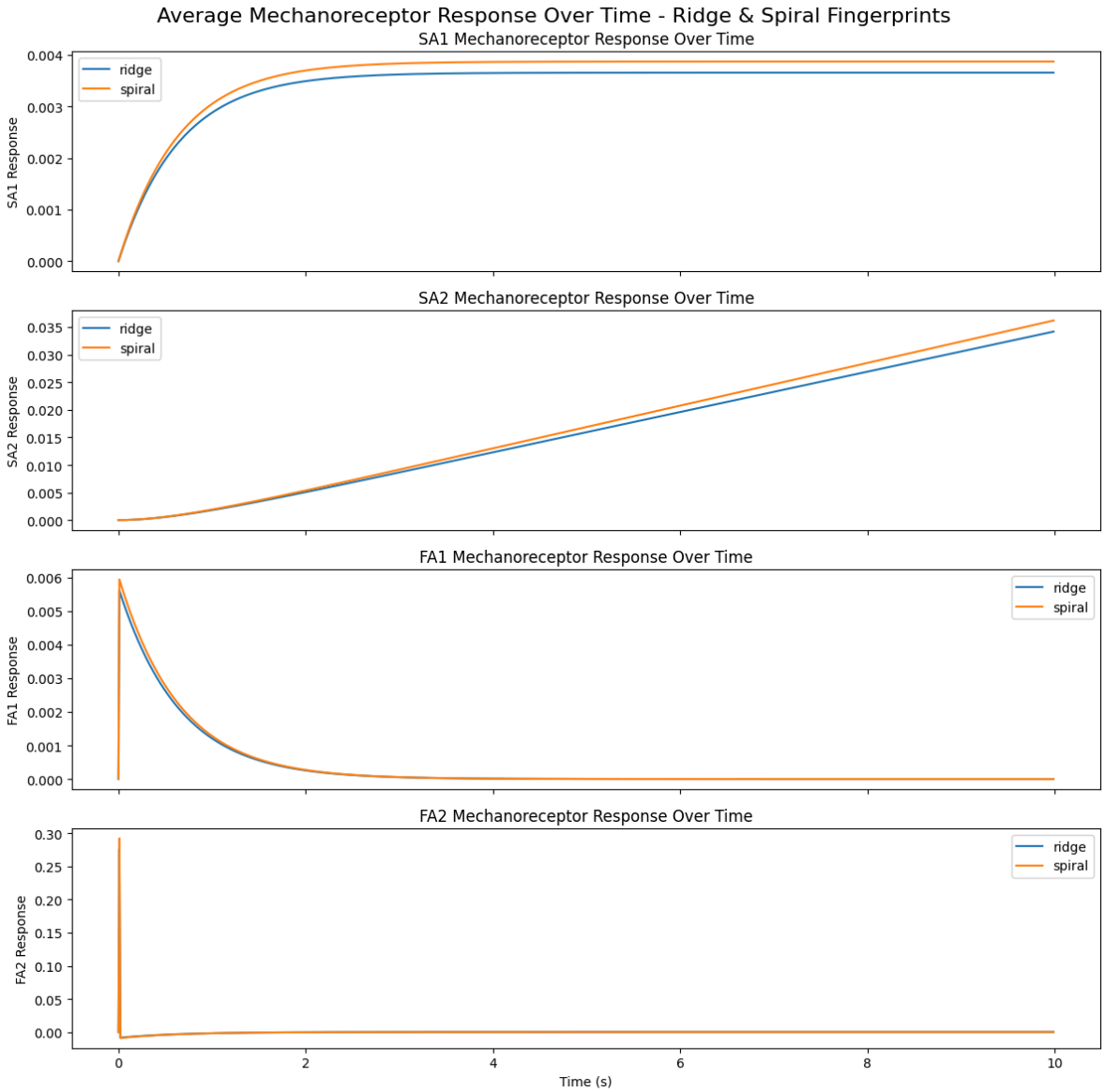

Figure 8. The global receptor responses for each mechanoreceptor for the ridge and spiral surface profile with the circular pressure map.

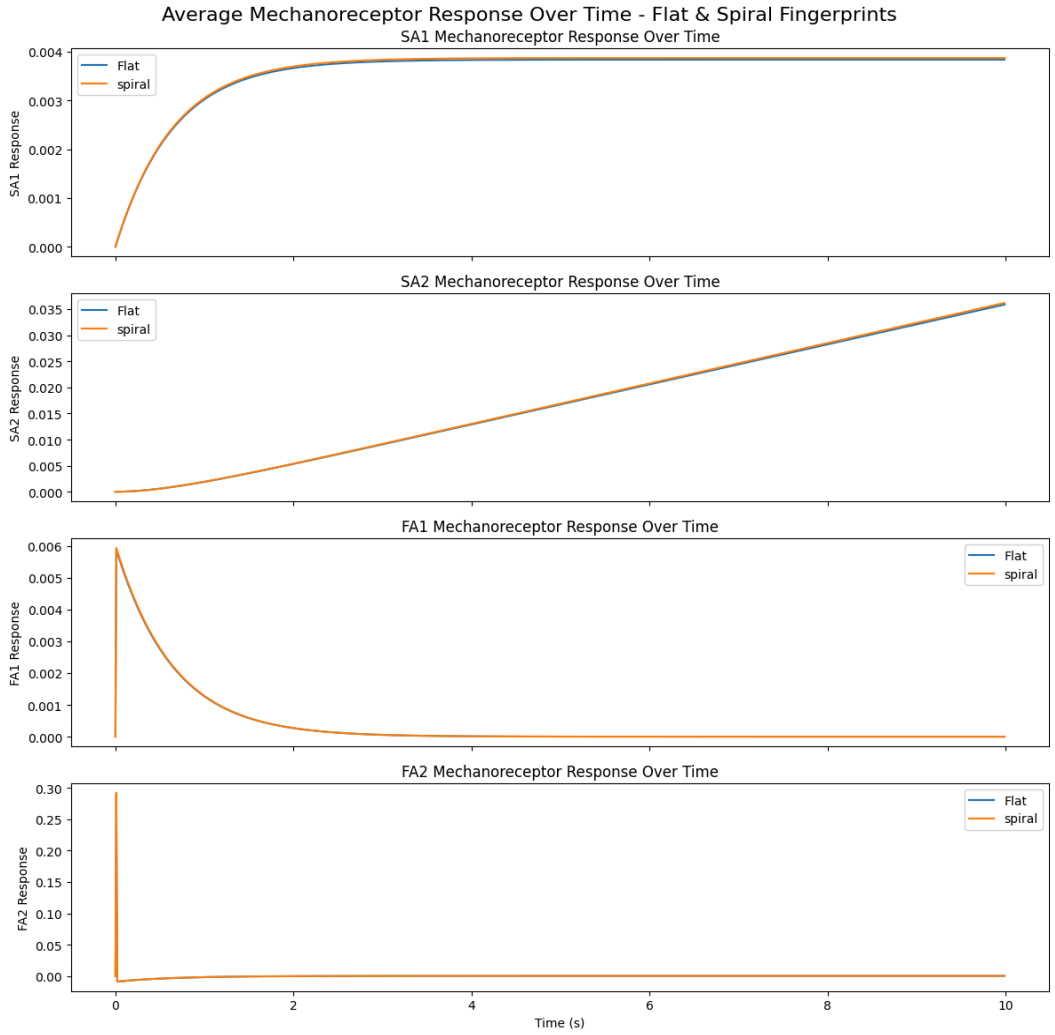

Figure 9. The global receptor responses for each mechanoreceptor for the flat and spiral surface profile with the circular pressure map.

As shown in the graphs above, the SA receptors are active depending on the pressure applied to the surface. As the pressure stabilizes, the SAI response also stabilizes. However, the response for SAII begins to climb due to the formula chosen for the SAII response calculations. This is likely not accurate to reality as both receptors are supposed to reach a maximum after some duration of time when constant pressure is held.

For the FA receptors, the responses are more accurate as they only spike when the pressure is being applied. For the FAI receptors, the response peaks at the initial introduction of the pressure map onto the surface profile. This decreases as the pressure continues to stabilize.

However, for the FAII receptor response, the signal is more drastic. This sharply returns to zero after the initial spike, which matches the theoretical behaviour.

Comparing the receptor responses with other surface profiles in Figures 8 and 9 also reveals some differences. The response for the flat surface profile is lower compared to the spiral, which is expected as the ridge improves the receptor's ability to pick up the pressure signal due to the curvature. This is seen to a greater extent in the graph in Figure 9 between the ridge pattern and the spiral pattern. The spiral pattern also beats the ridge pattern in amplifying the receptor signal. This can be explained due to the omnidirectional nature of a spiral compared to a ridge-like pattern in one dimension. This allows for the curvature to be greater, resulting in a larger amplification.

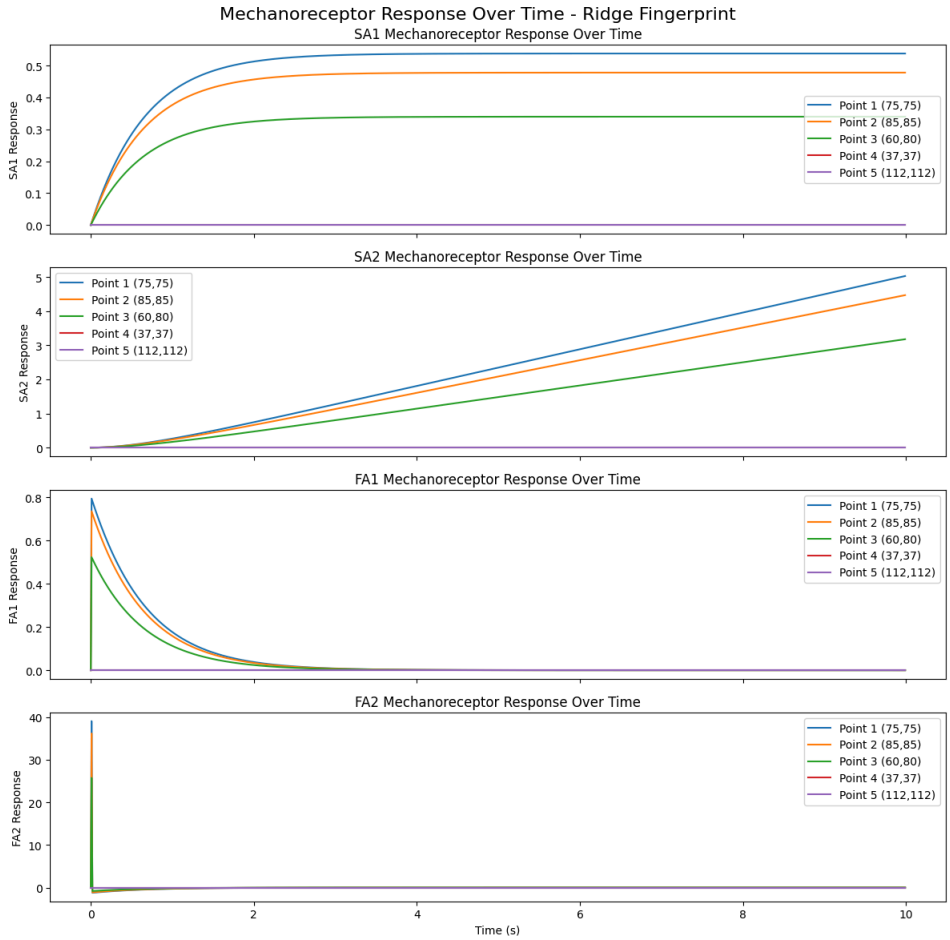

Figure 10. The receptor response of specific points on the ridge-like surface under a circular pressure map.

When simulating the indentation of skin selecting relevant parameters was a notable challenge. From the literature, the values of Young's modulus and the viscosity coefficient were selected to be 1.54 MPa and 1.0 Pa·sec inferred from the range of values used to describe the skin on one's fingertips. With each parameter subject to extreme variability as a result of many factors including hydration levels, temperature, humidity and age amongst others it was deemed necessary to prove the validity of our simulations by testing them on a variety of parameters to ensure the results follow expected trends.

Firstly, in Figure 9, the viscosity coefficient is set to the previously established standard of 1.0 Pa·sec and then swept Young's modulus value from 1.0 to 2.0 MPa over 5 uniformly distributed points. The resulting graph shows that for SAI receptors as Young's modulus increases and thus as the skin gets stiffer there is less overall deformation. This matches the theory as SAI receptors respond while deformation is occurring and in the case of stiffer skin, this will plateau sooner than examples with a lower Young's modulus. A similar theory is true for SAII receptors which respond to stretching, the plot with the highest Young's modulus showcases the least amount of SAII response as it resists stretching motions to a much higher degree than counterparts with a lower modulus that are less stiff.

FAI responses follow a largely similar trend in responding to dynamic skin deformation. It would be expected that data with a higher Young's modulus would deform less under the same amount of pressure and as such observe less receptor response as seen in the plot, thus proving the trend. Finally, FAII responses exhibit virtually the same behaviour across all modulus values. This is slightly unexpected as it would be expected to observe a large FAII response from data with a lower Young's modulus as it would not dampen oscillations as much during the simulation. Alongside this, negative results are also observed following the initial peak, this is quite unusual and could be the result of an issue in numerical calculations propagating throughout the FAII simulation.

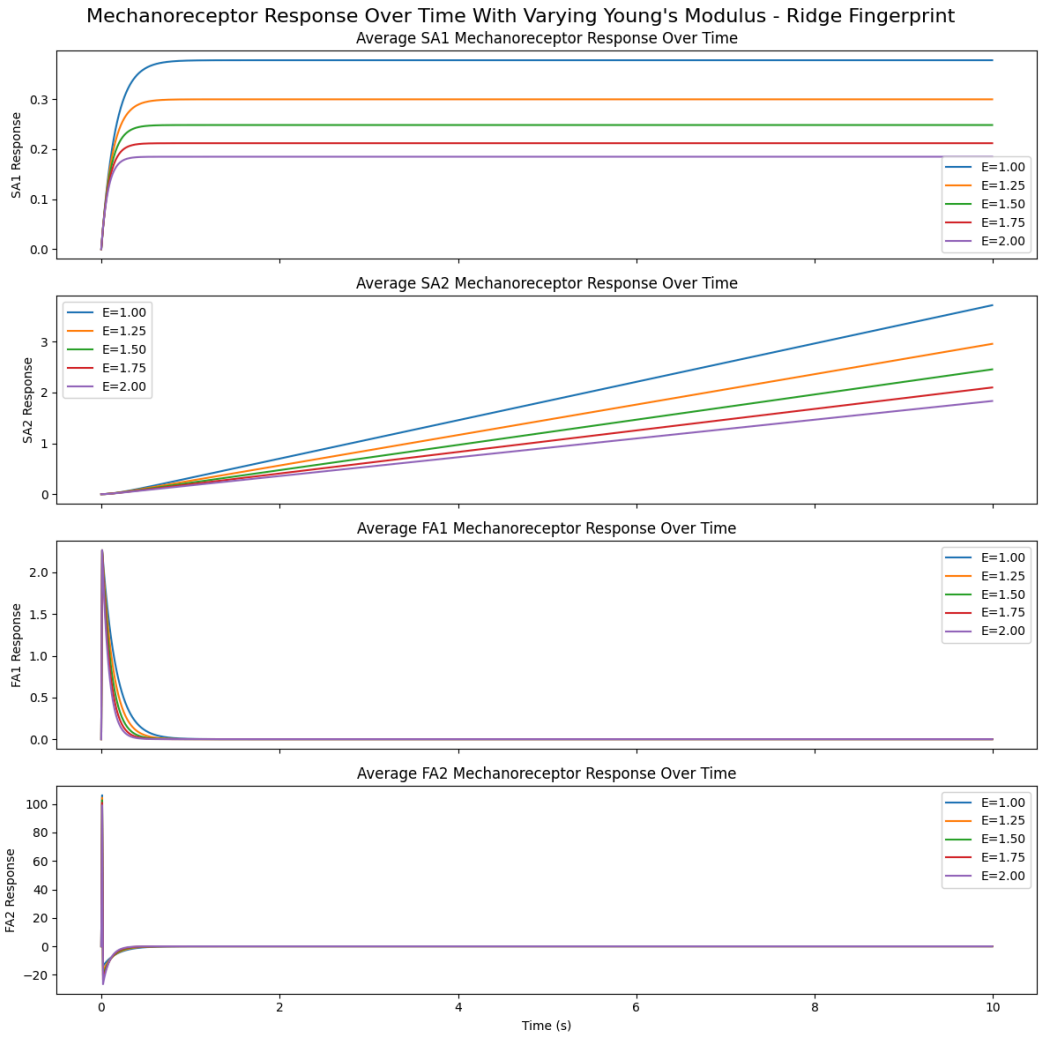

Figure 11. The average mechanoreceptor response as a function of time with Young's modulus variation between 1.0 and 2.0.

In Figure 12, a similar experiment to what was previously done for Figure 11 was attempted, but instead held Young's modulus at a constant of 1.54 MPa and varied the viscosity coefficient. The viscosity coefficient value varied from 0.1 to 1.0 Pa·sec over 5 uniformly distributed points. Firstly, with SAI response it is observed that values with a lower viscosity coefficient observe a large magnitude of receptor response, this aligns with the theory as a less viscoelastic surface would not dampen the response of sustained pressure more resulting in more receptor response as observed. The same is true for SAII response, the plots with a higher viscoelasticity coefficient dampen the response of the stretching input and thus showcase less

overall response magnitude. Next, FAI showcases response to dynamic pressure changes and that having a less viscoelastic material responds extremely well to input. This is observed on the graph where as the viscoelastic coefficient is decreased there is a distinct increase in receptor response as expected. Finally, FAII responds to high-frequency vibrations and in a similar vein to FAI, data with a smaller viscoelastic coefficient provides a much larger response than data with a high coefficient as a result of less dampening effects on the signal. However, the model does observe some unexpected behaviour with a viscosity coefficient of 0.1 where negative values can be observed. Unlike in Figure 11, these negative response values are isolated to only this one instance but do indicate a potential concern with the mathematical calculations of the FAII response.

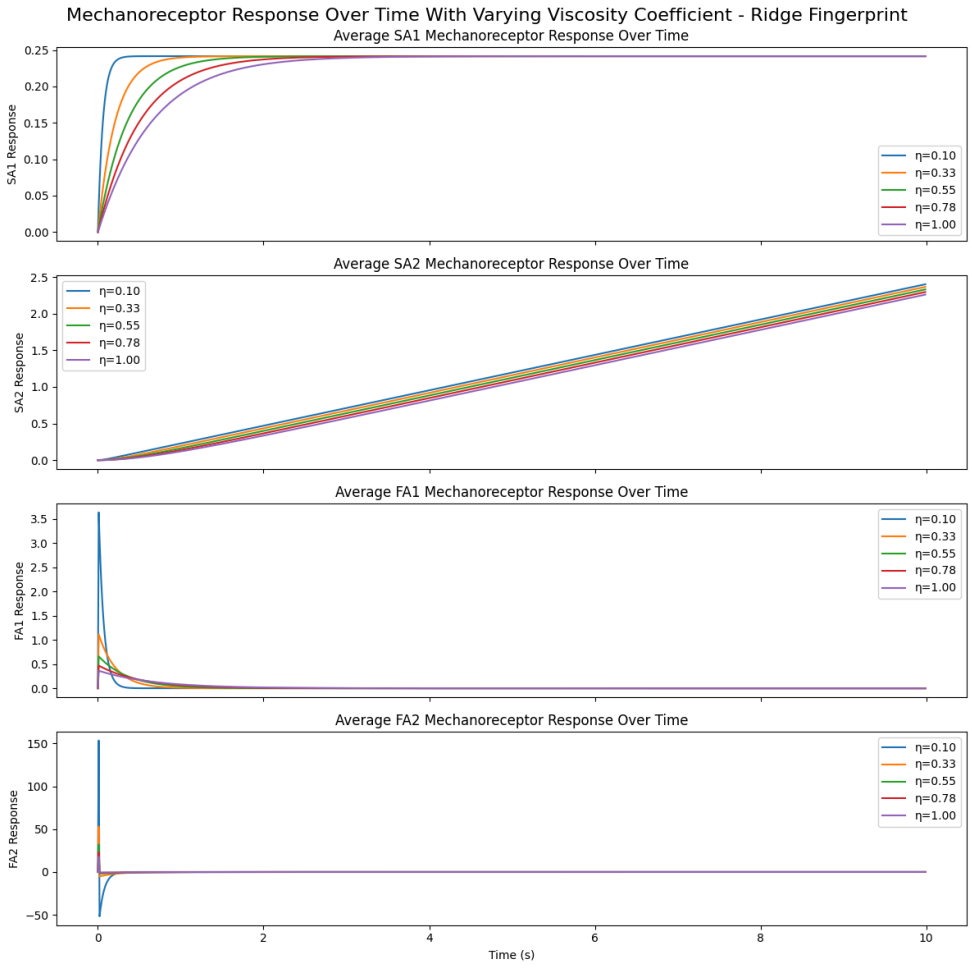

Figure 12. The average mechanoreceptor response as a function of time with an elasticity coefficient variation between 0.1 and 1.0.

5. Summary

The simulation uses the Kelvin-Voigt model to analyze the deformation of the skin under pressure. The simulation generates different fingertip ridge structures using Perlin noise to allow for a natural representation of fingertip texture. Pressure map patterns of circular, linear, and point based forces were applied to these ridge structures to evaluate differences in responses in mechanoreceptor activation over time.

The results obtained from the simulation validate what is expected from theoretical models. The SA receptor response was shown to have a constant response to stimuli while the FA receptor response was shown to activate only under initial stimuli and then not respond shortly after. In addition, the FAI receptors show a dynamic response to stimuli while FAII receptors show a discrete response, which matches with theory. Young's Modulus and viscoelasticity of different values were also simulated to show the influence of these properties relative to the mechanoreceptor response.

The overall simulations showed the impact of the fingertip ridge structure with respect to the mechanoreceptor response and displacement. When observing receptor responses resulting values largely followed all expected trends, thus validating the working principle of the simulation. However, FAII receptor responses presented potential concern as receptor responses were at times negative. This represents a potential calculation error in the model but appears to be only isolated to FAII responses. The identified issue would be evaluated further and fixed in future iterations of the model.

References

[1] Handler, A., & Ginty, D. D. (2021). The mechanosensory neurons of touch and their mechanisms of activation. *Nature Reviews Neuroscience*, *22*(9), 521-537. https://doi.org/10.1038/s41583-021-00489-x

[2] Prevost, A., Scheibert, J., & Debrégeas, G. (2009). Effect of fingerprint orientation on skin vibrations during tactile exploration of textured surfaces. *ArXiv*. https://doi.org/10.48550/arXiv.0911.3226

[3] Salehi, S., Cabibihan, J., & Ge, S. S. Artificial Skin Ridges Enhance Local Tactile Shape Discrimination. *Sensors*, *11*(9), 8626-8642. https://doi.org/10.3390/s110908626

[4] Corniani, G., Lee, Z. S., Carré, M. J., Lewis, R., Delhaye, B. P., & Saal, H. P. (2024). Sub-surface deformation of individual fingerprint ridges during tactile interactions. eLife Sciences Publications, Ltd. https://doi.org/10.7554/elife.93554.1

[5] Scheibert, J., Leurent, S., & Prevost, A. (2009). The Role of Fingerprints in the Coding of Tactile Information Probed with a Biomimetic Sensor. *Science*. https://doi.org/10.1126/science.1166467

[6] Bilaloglu, S., Lu, Y., Geller, D., Rizzo, J. R., Aluru, V., Gardner, E. P., & Raghavan, P. (2015). Effect of blocking tactile information from the fingertips on adaptation and execution of grip forces to friction at the grasping surface. *Journal of Neurophysiology*, *115*(3), 1122. https://doi.org/10.1152/jn.00639.2015

[7] V. Maheshwari, Class Lecture, Topic: “Tactile Sensors: Lecture 7.” NE466, University of Waterloo, Faculty of Engineering, Jan. 2025.

[8] V. Maheshwari, Class Lecture, Topic: “Tactile Sensors: Lecture 2.” NE466, University of Waterloo, Faculty of Engineering, Jan. 2025.

[9] Iheanacho F, Vellipuram AR. Physiology, Mechanoreceptors. [Updated 2023 Sep 4]. In: StatPearls [Internet]. Treasure Island (FL): StatPearls Publishing; 2025 Jan-. Available from: https://www.ncbi.nlm.nih.gov/books/NBK541068/

[10] V. Maheshwari, Class Lecture, Topic: “Tactile Sensors: Lecture 3.” NE466, University of Waterloo, Faculty of Engineering, Jan. 2025.

[11] Michael Kücken, Alan C. Newell, Fingerprint formation, Journal of Theoretical Biology, Volume 235, Issue 1, 2005, Pages 71-83, ISSN 0022-5193, https://doi.org/10.1016/j.jtbi.2004.12.020.

[12] V. Maheshwari, Class Lecture, Topic: “Tactile Sensors: Lecture 5.” NE466, University of Waterloo, Faculty of Engineering, Jan. 2025.

[13] Kijak, E., Margielewicz, J., & Pihut, M. (2020). Identification of Biomechanical Properties of Temporomandibular Discs. In E. Winocur (Ed.), Pain Research and Management (Vol. 2020, pp. 1–11). Hindawi Limited. https://doi.org/10.1155/2020/6032832

[14] Hildick-Smith, G. (2024, December 16). *Perlin Noise: the ground-breaking tool in procedural generation*. The Bubble. https://www.thebubble.org.uk/current-affairs/science-technology/perlin-noise-the-ground-breaking-tool-in-procedural-generation/

[15] Kalra, A., & Lowe, A. (2016). An Overview of Factors Affecting the Skins Youngs Modulus. In Journal of Aging Science (Vol. 4, Issue 2). OMICS Publishing Group. https://doi.org/10.4172/2329-8847.1000156

[16] NE 466 Winter 2025 Group 5, Skin Ridge Model, (2025), GitHub repository, https://github.com/CydiaBoss/skin-ridge-model

[17] Adams Michael J., Johnson Simon A., Lefèvre Philippe, Lévesque Vincent, Hayward Vincent, André Thibaut and Thonnard Jean-Louis, (2013), Finger pad friction and its role in grip and touch. J. R. Soc. Interface. http://doi.org/10.1098/rsif.2012.0467

[18] Walsh, C., O'Connor, D., & Doran, M. (2017). An Overview of Factors Affecting the Skin's Young's Modulus. *Journal of Materials Science*, 32(2). https://doi.org/10.4172/2329-8847.1000156

[19] Yousef H, Alhajj M, Fakoya AO, et al. Anatomy, Skin (Integument), Epidermis. [Updated 2024 Jun 8]. In: StatPearls [Internet]. Treasure Island (FL): StatPearls Publishing; 2025 Jan-. Available from: https://www.ncbi.nlm.nih.gov/books/NBK470464/